L-moments of the Birnbaum-Saunders distribution and its extreme value version: Estimation, goodness of fit and application to earthquake data

Camilo Lillo[1], Víctor Leiva[2,3], Orietta Nicolis[1], Robert G. Aykroyd[4]

[1]Institute of Statistics, Universidad de Valparaíso, Chile

[2]Faculty of Engineering and Sciences, Universidad Adolfo Ibáñez, Chile

[3]Faculty of Administration, Accounting and Economics, Universidade Federal de Goiás, Goiânia, Brazil

[4]Department of Statistics, University of Leeds, UK

Understanding patterns in the frequency of extreme natural events, such as earthquakes, is important as it helps in the prediction of their future occurrence and hence provides better civil protection. Distributions describing these events are known to be heavy tailed and positive skew making standard distributions unsuitable for such a situation. The Birnbaum-Saunders distribution and its extreme value version have been widely studied and applied due to their attractive properties. We derive L-moment equations for these distributions and propose novel methods for parameter estimation, goodness-of-fit assessment and model selection. A simulation study is conducted to evaluate the performance of the L-moment estimators, which is compared to that of the maximum likelihood estimators, demonstrating the superiority of the proposed methods. To illustrate these methods in a practical application, a data analysis of real-world earthquake magnitudes, obtained from the global centroid moment tensor catalogue during 1962-2015, is carried out. This application identifies the extreme value Birnbaum-Saunders distribution as a better model than classic extreme value distributions for describing seismic events.

Keywords: GCMT catalogue; Generalized extreme value distributions; goodness-of-fit methods; maximum likelihood and moment estimation; Monte-Carlo simulation; R software.

1. Introduction

Every scientific investigation can be thought of as sampling from a random variable (RV) associated with some statistical distribution. One of the ubiquitous challenges of distributional analysis is to reduce these data to a few relevant numbers without significant loss of information. This reduction can be made by computing quantiles associated with order statistics, or by other distributional metrics, as conventional moments (called here C-moments and denoted as CM) [47]. In geosciences, data from the same variable are measured at different locations to estimate their common statistical distribution.

A distribution can be characterized using CM through the mean, standard deviation (SD), coefficients of variation (CV), skewness (CS) and kurtosis (CK). These moments may also be used for estimation and goodness-of-fit (GOF) assessment. However, it is well known that the CM have limitations when applied to data with high variation, heavy tails and departures from symmetry. To avoid these limitations, an alternative to the CM was introduced, with similar interpretations and applications, named L-moments (LM)

Corresponding author: Víctor Leiva. Email: victorleivasanchez@gmail.com. URL: www.victorleiva.cl

[13]. In contrast to CM, LM are defined as the expected value of linear combinations of order statistics. These can be used to obtain quantities similar to the conventional SD, CV, CS and CK, named L-SD, L-CV, L-CS and L-CK, respectively [13]. It is also possible to define standardized LM, known as LM ratios, analogous to the standardized CM. As with CM, LM and LM ratios can be used for parameter estimation and GOF assessment.

Challenges posed by extreme events are of interest in different areas. According to [50], the LM theory can be considered one of the most significant recent advances related to the understanding of such events. Standardized LM have been used for goodness of fit in different extreme events [19, 21, 36].

LM have several advantages over CM. For example, LM GOF assessment is easy to use and has powerful features for discriminating between distributions. In addition, LM estimators are unbiased, robust and have standard errors (SE) smaller than other estimators [7]. These advantages are particularly important with data which have high variability or skewness, as well as heavy tails, that is, under non-normality. Data that frequently present these characteristics are endemic in the geosciences, and in particular in earthquake data. Applications of LM is not limited to these sciences. There exist areas as diverse as finance and reliability where LM have been applied [13, 48].

The Birnbaum-Saunders (BS) distribution has been extensively studied and applied across a wide range of scientific areas because of its good properties [3], [14, pp. 651-663], [23, 28–30, 32–34, 43, 53]. The BS distribution can be used to model many types of unimodal data that take values greater than zero and are positive skew. [27] provided a theoretical justification to why the BS distribution is a suitable model for describing environmental data. For some applications of the BS distribution in earth and environmental sciences, the interested reader is referred to, for example, [9, 12, 20, 24–26, 38, 44, 49].

The BS distribution has its origins in the theory of material fatigue. It is accepted that fatigue is produced by cumulative damage. It starts with an imperceptible fissure in the material provoked by stress, which is propagated through the material until a critical threshold is reached, causing its fracture or failure. It has been shown that such cumulative processes are well described by the BS distribution [3, 34].

Several phenomena, such as earthquakes, evolve in a similar manner to fatigue; see [35] for an analogy in neural activity. Indeed, fatigue is created from vibrations and an earthquake can be thought of similarly. It is accepted that earthquakes are produced by the accumulation of energy, beginning with the deformation of rocks induced by the movement of tectonic plates, where the geological fault is located; see [10] and references therein for more details about the physical laws describing the generation of earthquakes. This deformation grows due to the energy accumulated by stress, provoking the rupture of rocks, when this energy exceeds a critical threshold, which releases the energy. The difference between fatigue and earthquake generation is that in fatigue the failure occurs when the threshold is reached, whereas in an earthquake the release of energy generates seismic waves that produce the event. Therefore, the BS distribution seems to be a good candidate to model earthquake data. However, as mentioned, earthquakes correspond to extreme events. Then, we need to use an extreme value (EV) version of the BS distribution (EVBS), which was derived by [9].

Extreme value distributions have been used in seismology as it is assumed that the distribution of earthquake magnitudes follows the Gutenberg-Richter law [41], which is equivalent to the two-parameter exponential (EXP) distribution. The generalized Pareto (GP) distribution extends the EXP distribution, and hence the GP distribution allows an improved modelling of these magnitudes [45]. When modelling annual maximum earthquake magnitudes, the Gumbel (GU) distribution is analogous to the EXP distribution [45], whereas the generalized extreme value (GEV) distribution extends the GU distribu-

tion in the setting of maximum magnitudes [45]. Recent work on statistical distributions proposed for modelling earthquake is attributed to [10]. Note that no applications of BS distributions in seismology have yet been considered.

The main objectives of this paper for the BS and EVBS distributions are: (i) to derive LM equations, (ii) to propose LM estimators and evaluate their performance, (iii) to provide GOF assessment using LM, and (iv) to apply these results to real-world earthquake data. The proposed methods are evaluated using Monte Carlo (MC) simulations and applied to annual maximum earthquake magnitude data taken from the global centroid moment tensor (GCMT) catalogue.

The rest of the paper is organized as follows. Section 2 presents background to the BS and EVBS distributions. Section 3 derives the LM of these distributions and proposes estimation and GOF methods. Section 4 provides the numerical results, first by checking properties with simulations and, second, by illustrating them with real-world earthquake data. Finally, Section 5 presents the conclusions as well as discussing possible future research.

2.   Background

In this section, we introduce some preliminary aspects related to BS and EVBS distributions.

2.1   *The BS distribution*

The BS distribution is defined in terms of the standard normal distribution by means of the RV $T = \beta(\alpha Z/2 + \sqrt{(\alpha Z/2)^2 + 1})^2$, where $Z \sim \mathrm{N}(0,1)$, α is a shape parameter and β is a scale parameter, as well as the median of T. This is denoted by $T \sim \mathrm{BS}(\alpha, \beta)$ and the corresponding probability density function (PDF) is

$$f_T(t; \alpha, \beta) = \frac{1}{\sqrt{2\pi}} \exp\left(-\frac{1}{2\alpha^2}\left(\frac{t}{\beta} + \frac{\beta}{t} - 2\right)\right)\frac{t^{-3/2}(t+\beta)}{2\alpha\sqrt{\beta}}, t > 0, \alpha > 0, \beta > 0. \quad (1)$$

Some properties of $T \sim \mathrm{BS}(\alpha, \beta)$ are: (A1) $cT \sim \mathrm{BS}(\alpha, c\beta)$, for $c > 0$; (A2) $1/T \sim \mathrm{BS}(\alpha, 1/\beta)$; (A3) $Z = (\sqrt{T/\beta} - \sqrt{\beta/T})/\alpha \sim \mathrm{N}(0, 1)$, and (A4) $V = (T/\beta + \beta/T - 2)/\alpha^2 \sim \chi^2(1)$, that is, V follows the χ^2 distribution with one degree of freedom. Furthermore, the mean and variance of T are $\mathrm{E}(T) = \beta(1 + \alpha^2/2)$ and $\mathrm{Var}(T) = \alpha^2\beta^2(1 + 5\alpha^2/4)$, respectively. The BS PDF, shown in equation (1), can be written as $f_T(t; \alpha, \beta) = \phi(a(t))A(t)$, for $t > 0$, where ϕ is the standard normal PDF, $a(t) = a(t; \alpha, \beta) = (1/\alpha)(\sqrt{t/\beta} - \sqrt{\beta/t})$, and $A(t) = A(t; \alpha, \beta) = \mathrm{d}a(t)/\mathrm{d}t = t^{-3/2}(t+\beta)/(2\alpha\sqrt{\beta})$.

Figure 1 shows graphs of the BS PDF given in equation (1) for $\beta = 1.0$, without loss of generality, and for values of $\alpha \in \{0.1, 0.5, 1.0, 2.0, 4.0\}$. From this figure, note that the BS distribution is continuous, unimodal and positively skewed (asymmetry to the right). Also, note that, as α goes to zero, the BS distribution become symmetric around β (the median of the distribution) and its variability decreases. In addition, as α increases, the distribution tends to be more asymmetric, with a similar shape to the EXP distribution when $\alpha = 4.0$. Thus, α not only controls the shape, but also the skewness and kurtosis of the distribution.

The BS cumulative distribution function (CDF) is $F_T(t; \alpha, \beta) = \Phi(a(t))$, for $t > 0$, where Φ is the standard normal CDF, whereas the BS quantile function (QF) is

$$t(q; \alpha, \beta) = F_T^{-1}(q) = \beta\big(\alpha z(q)/2 + \sqrt{(\alpha z(q)/2)^2 + 1}\big)^2, \quad 0 < q < 1, \quad (2)$$
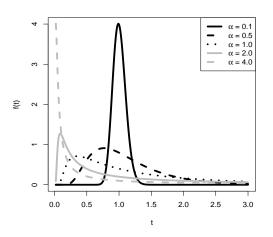
3

Figure 1. PDF Plots of the BS distribution for $\beta = 1.0$ and the indicated value of α.

where $z \equiv \Phi^{-1}$ is the standard normal QF, with Φ^{-1} being the inverse function of the standard normal CDF.

2.2 The EVBS distribution

To define the EVBS distribution, the relationship between $T \sim \text{BS}(\alpha, \beta)$ and $Z \sim \text{N}(0, 1)$, given in equation (1), is relaxed allowing Z to follow a GEV distribution. The GEV distribution depends on a parameter $\xi \in \text{R}$, known as the EV index, which is also a shape parameter determining the tail behaviour of the distribution [6]. Thus, one of the EVBS distributions proposed by [9], to deal with data of maxima, is denoted as $X \sim \text{EVBS}(\alpha, \beta, \xi)$, whose PDF is expressed as $f_X(x; \alpha, \beta, \xi) = g(a(x); \xi)A(x)$. Here, $g(u; \xi) = \text{d}G(u; \xi)/\text{d}u$, with $u \in \text{R}$, where

$$G(u; \xi) = \begin{cases} \exp(-(1 + \xi y)^{-1/\xi}), & \text{if } \xi \neq 0 \text{ and } 1 + \xi x > 0; \\ \exp(-\exp(-y)), & \text{if } \xi = 0. \end{cases} \tag{3}$$

Note that equation (3) is the unique non-degenerate limiting CDF of the sequence of maxima for a deterministic number k, with $k \to \infty$, in either independent and identically distributed or weakly dependent and stationary RV cases. From the CDF given in equation (3), observe that the GU distribution is a particular case when $\xi = 0$. The CDF of $X \sim \text{EVBS}(\alpha, \beta, \xi)$ is

$$F_X(x; \alpha, \beta, \xi) = \begin{cases} \exp(-(1 + \xi a(x))^{-1/\xi}), & \text{if } \xi \neq 0 \text{ and } 1 + a(x)\xi > 0; \\ \exp(-\exp(-a(x))), & \text{if } \xi = 0; \end{cases} \tag{4}$$

4

and the corresponding PDF is

$$
f_X(x; \alpha, \beta, \xi) = \begin{cases} \frac{1}{2x\alpha} \exp\left(-\left(\frac{\xi}{\alpha}\left(\sqrt{\frac{x}{\beta}} - \sqrt{\frac{\beta}{x}}\right) + 1\right)^{-\frac{1}{\xi}}\right) \left(\frac{\xi}{\alpha}\left(\sqrt{\frac{x}{\beta}} - \sqrt{\frac{\beta}{x}}\right) + 1\right)^{-\frac{\xi+1}{\xi}} \\ \times \left(\sqrt{\frac{\beta}{x}} + \sqrt{\frac{x}{\beta}}\right), \text{if } \xi \neq 0; \\ \frac{1}{2x\alpha} \exp\left(\frac{1}{\alpha}\left(\sqrt{\frac{\beta}{x}} - \sqrt{\frac{x}{\beta}}\right) - \exp\left(\frac{1}{\alpha}\left(\sqrt{\frac{\beta}{x}} - \sqrt{\frac{x}{\beta}}\right)\right)\right) \left(\sqrt{\frac{\beta}{x}} + \sqrt{\frac{x}{\beta}}\right), \\ \text{if } \xi = 0; \end{cases}
$$

which is defined for $x > (\alpha^2\beta + 2\beta\xi^2)/(2\xi^2) - \sqrt{(\alpha^4\beta^2 + 4\alpha^2\beta^2\xi^2)/\xi^4}/2$, if $\xi > 0$; for $x > 0$, if $\xi = 0$; and for $0 < x < (\alpha^2\beta + 2\beta\xi^2)/(2\xi^2) + \sqrt{(\alpha^4\beta^2 + 4\alpha^2\beta^2\xi^2)/\xi^4}/2$, if $\xi < 0$. As in the GEV case, from equation (4) we obtain a Birnbaum-Saunders-Gumbel (BSGU) distribution when $\xi = 0$. Figure 2 shows graphs of the EVBS PDF given in equation (4) for values of $\alpha \in \{0.1, 0.5, 1.0, 1.5, 2.0, 4.0\}$ and $\xi \in \{-1, -0.5, 0, 0.5, 1.0\}$, and without loss of generality $\beta = 1.0$. Note that the EVBS distribution is very flexible with a unimodal or bimodal behavior (depending on the values of ξ) and a positive or negative skew. When α is small, the asymmetry of the distribution depends on the values assumed for ξ (for example, if ξ is negative, the distribution is skewed to the left). In addition, when α increases, the distribution is skewed to the right (regardless of the value assumed for ξ). Changes in the value of the kurtosis depend on the value assumed for ξ [26].
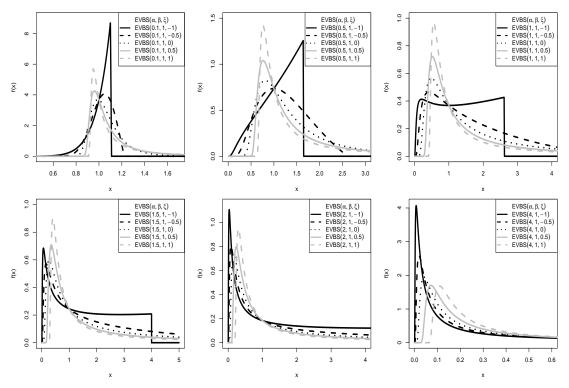

Figure 2. PDF plots of the EVBS distribution for $\beta = 1.0$ and the indicated values of (α, ξ).

The EVBS distribution for minima, proposed in [9], is denoted by $X \sim \text{EVBS}^*(\delta, \beta, \xi)$. Thus, for left tail, we write equation (4) with a limiting CDF $G^*(u; \xi) = 1 - G(-u; \xi)$,

where G is defined in equation (3). Then, the CDF of $X \sim \text{EVBS}^*(\delta, \beta, \xi)$ is

$$
F_X^*(x; \alpha, \beta, \xi) = \begin{cases} 1 - \exp(-(1 + \xi a(x))^{-1/\xi}), & \text{if } \xi \neq 0 \text{ and } 1 + \xi > 0, x > 0; \\ 1 - \exp(-\exp(-a(x))), & \text{if } \xi = 0, x > 0. \end{cases} \tag{5}
$$

For the EVBS and EVBS* distributions, α is a shape parameter, β is a scale parameter and ξ is also a shape parameter, but with ξ determining the right-tail behaviour of the EVBS distribution or the left-tail behaviour of the EVBS* distribution. Properties (A1) and (A2) of the BS distribution are also valid for the EVBS* and EVBS distributions, whose CM are mentioned in [26]. Also, it is possible to obtain BSGU and BSGU* distributions for minima and maxima, respectively. The QF of the EVBS distribution is

$$
x(q; \alpha, \beta, \xi) = F^{-1}(q) = \beta\left(\alpha z_1(q)/2 + \sqrt{(\alpha z_1(q)/2)^2 + 1}\right)^2, \quad 0 < q < 1, \tag{6}
$$

where $z_1(q) = ((-\log(q))^{-\xi} - 1)/\xi$, if $\xi \neq 0$, or $z_1(q) = -\log(-\log(q))$, if $\xi = 0$. For the EVBS* distribution, the QF is obtained replacing $z_1(q)$ by $-z_1(1 - q)$ in equation (6). Figure 3 shows graphs of the EVBS* PDF given in equation (5) for values of $\alpha \in \{0.1, 0.5, 1.0, 1.5, 2.0, 4.0\}$, of $\xi \in \{-1, -0.5, 0, 0.5, 1.0\}$ and, without loss of generality, $\beta = 1.0$. From this figure, note that the EVBS* distribution can be unimodal or bimodal, depending on the values of ξ. Observe that, if α is small, the skewness of the distribution depends on the value assumed for ξ (differently to what occurs with the EVBS distribution). As ξ increases, the distribution is heavy left tailed. When α increases, the distribution is asymmetric to the right, regardless of the ξ value.
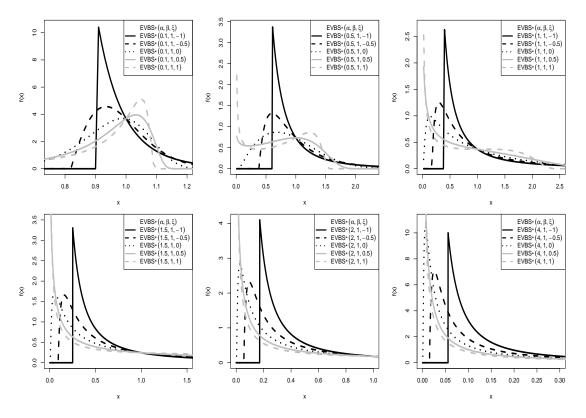

Figure 3. PDF plots of the EVBS* distribution for $\beta = 1.0$ and the indicated values of (α, ξ).

3. Theoretical results

In this section, we derive the LM of BS and EVBS distributions and propose estimation and GOF methods based on these LM.

3.1   *L-moments*

In general, the first four LM of a continuous probability distribution are defined as

$$\lambda_1 = \int_0^1 x(q)\mathrm{d}q, \quad \lambda_2 = \int_0^1 x(q)(2q-1)\mathrm{d}q,$$

$$\lambda_3 = \int_0^1 x(q)(6q^2 - 6q + 1)\mathrm{d}q, \quad \lambda_4 = \int_0^1 x(q)(20q^3 - 30q^2 + 12q - 1)\mathrm{d}q, \qquad (7)$$

where $x(q)$ is the corresponding $100 \times q$th quantile. The first LM, λ_1, is the mean of the distribution, and the second LM, $\lambda_2 > 0$, is a scale measure. The LM ratios defined as

$$\tau_r = \frac{\lambda_r}{\lambda_2}, \quad r = 3, 4, \qquad (8)$$

are dimensionless measures of the distribution shape. Analogously to the CM, the L-CS, τ_3, is a measure of skewness, with $0 \le \tau_3 \le 1$. The L-CK, τ_4, is a measure of kurtosis, with $(5\tau_3^2 - 1)/4 \le \tau_4 \le 1$. The LM ratio $\tau = \lambda_2/\lambda_1$ is the analogue of the conventional CV and corresponds to the L-CV, where $0 < \tau < 1$ for distributions with positive support.

The sample LM are computed from the order statistics $X_{1:n} \le \cdots \le X_{n:n}$ as

$$l_1 = b_0 = \frac{1}{n}\sum_{i=1}^n X_{i:n}, \quad l_2 = 2b_1 - b_0,$$

$$l_3 = 6b_2 - 6b_1 + b_0, \quad l_4 = 20b_3 - 30b_2 + 12b_1 - b_0, \qquad (9)$$

where

$$b_r = \frac{1}{n}\sum_{i=r+1}^n (i-1)(i-2)\cdots(i-r)\frac{X_{i:n}}{(n-1)(n-2)\cdots(n-r)}, \quad r = 1, 2, 3.$$

The calculation of sample LM is implemented in the `R` software by the command `Lcoefs` of the `Lmoments` package [17, 18].

Specific LM equations of the BS, EVBS and EVBS* distributions can be obtained by substituting their corresponding QF into equation (7). In particular, for the BS distribution, its first four LM are

$$\lambda_1^{\mathrm{BS}} = \beta\left(1 + \frac{\alpha^2}{2}\right), \quad \lambda_2^{\mathrm{BS}} = 2\beta h_2,$$

$$\lambda_3^{\mathrm{BS}} = \frac{\beta\alpha^2\sqrt{3}}{2\pi}, \quad \lambda_4^{\mathrm{BS}} = \beta(20h_4 - 30h_3 + 12h_2), \qquad (10)$$

where

$$h_j = \int_0^1 q^{j-1}\alpha z(q)\sqrt{(\alpha z(q)/2)^2 + 1}\,\mathrm{d}q, \quad j = 1, 2, 3, 4. \qquad (11)$$

In the case of the EVBS and EVBS* distributions, closed forms for first four LM are

$$\lambda_1^{\text{EVBS}} = \begin{cases} \beta\left(\alpha^2(1+\Gamma(1-2\xi)-2\Gamma(1-\xi))/(2\xi^2)+h_1+1\right), & \text{if } \xi \neq 0; \\ \beta\left(17\pi\alpha^2/54+1+h_1\right), & \text{if } \xi = 0; \end{cases}$$

$$\lambda_2^{\text{EVBS}} = \begin{cases} \beta(\alpha^2((4^\xi-1)\Gamma(1-2\xi)+(2-2^{\xi+1})\Gamma(1-\xi))/(2\xi^2)+2h_2-h_1), & \text{if } \xi \neq 0; \\ \beta\left(32\pi\alpha^2/157+2h_2-h_1\right), & \text{if } \xi = 0; \end{cases}$$

$$\lambda_3^{\text{EVBS}} = \begin{cases} \beta\Big(\alpha^2((2(9^\xi)-3(4^\xi)+1)\Gamma(1-2\xi)-4(3^\xi)\Gamma(1-\xi)-3(2^{\xi+1})+2)/(2\xi^2) \\ \qquad +6h_3-6h_2+h_1\Big), & \text{if } \xi \neq 0; \\ \beta\left(\sqrt{22\pi}\alpha^2/15+6h_3-6h_2+h_1\right), & \text{if } \xi = 0; \end{cases}$$

$$\lambda_4^{\text{EVBS}} = \begin{cases} \beta\Big(\alpha^2\left(\Gamma(1-2\xi)\left(5(16^\xi)-10(9^\xi)+6(4^\xi)-1\right)-\Gamma(1-\xi)\left(5(2^{2\xi+1})-20(3^\xi)\right. \\ \qquad \left.+6(2^{\xi+1})-2\right)\right)/(2\xi^2)+20h_4-30h_3+12h_2-h_1\Big), & \text{if } \xi \neq 0; \\ \beta\left(11\pi^2\alpha^2/400+20h_4-30h_3+12h_2-h_1\right), & \text{if } \xi = 0; \end{cases} \tag{12}$$

and

$$\lambda_1^{\text{EVBS*}} = \begin{cases} \beta\left(\alpha^2(1+\Gamma(1-2\xi)-2\Gamma(1-\xi))/(2\xi^2)+h_1(\alpha,\xi)+1\right), & \text{if } \xi \neq 0; \\ \beta\left(17\pi\alpha^2/54+1+h_1\right), & \text{if } \xi = 0; \end{cases}$$

$$\lambda_2^{\text{EVBS*}} = \begin{cases} \beta(\alpha^2((1-4^\xi)\Gamma(1-2\xi)+(2^{\xi+1}-2)\Gamma(1-\xi))/(2\xi^2)+2h_2-h_1), & \text{if } \xi \neq 0; \\ \beta\left(32\pi\alpha^2/157+2h_2-h_1\right), & \text{if } \xi = 0; \end{cases}$$

$$\lambda_3^{\text{EVBS*}} = \begin{cases} \beta\Big(\alpha^2((2(9^\xi)-3(4^\xi)+1)\Gamma(1-2\xi)-4(3^\xi)\Gamma(1-\xi)-3(2^{\xi+1})+2)/(2\xi^2) \\ \qquad +6h_3-6h_2+h_1\Big), & \text{if } \xi \neq 0; \\ \beta\left(\sqrt{30}\alpha^2/\pi^2+6h_3-6h_2+h_1\right), & \text{if } \xi = 0; \end{cases}$$

$$\lambda_4^{\text{EVBS*}} = \begin{cases} \beta\Big(\alpha^2\left(\Gamma(1-2\xi)\left(10(9^\xi)+24(2^{2\xi})-15(2^{2\xi+1})-5(2^{4\xi})+1\right)-\Gamma(1-\xi)\left(5(2^{2\xi+1})+\right. \\ \qquad \left.-20(3^\xi)+3(2^{\xi+2})-2\right)\right)/(2\xi^2)+20h_4-30h_3+12h_2-h_1\Big), & \text{if } \xi \neq 0; \\ \beta\left(5\alpha^2\sqrt{447}/(4\pi^2)+20h_4-30h_3+12h_2-h_1\right), & \text{if } \xi = 0; \end{cases} \tag{13}$$

where, in equations (12) and (13), Γ is the gamma function and $\xi < 1/2$, such that $1-2\xi > 0$ in the argument of $\Gamma(1-2\xi)$. Note that h_j defined in equation (11), for $j = 1, 2, 3, 4$, used to compute the LM of the BS, EVBS and EVBS* distributions by equations (10), (12) and (13), have expressions for z and z_1 as given in equations (2) and (6), respectively. Also note that the L-CV, L-CS and L-CK of the BS, EVBS and EVBS* distributions do not depend on their scale parameter.

3.2 *Goodness-of-fit assessment based on L-moments*

Next, three GOF assessment methods based on LM are proposed. First, we describe a method known as the LM ratio chart, which has been widely used to select a suitable distribution. The LM ratio diagram allows us to represent the LM of different distributions in a single graphical plot. This graph is constructed using the known relationship between L-CK and L-CS for each distribution. In particular, the coordinate axes are (τ_3, τ_4), as defined in equation (8), with a line or region indicating the set of values of (τ_3, τ_4) permitted under the model. This plot is known as the τ_3-τ_4 chart and is analogous to the β_1-β_2 chart used in CM [25]. Distributions belonging to the location-scale family (for example, the normal distribution) are plotted as a single point on the diagram. Two-parameter distributions with scale and shape parameters (for example, the BS distribution) or three-parameter distributions with location, scale and shape parameters (for example, the GEV distribution) are plotted as a line, with different points on it corresponding to different values of the shape parameter. Distributions with more than one shape parameter (for example, the EVBS distribution) generally cover two-dimensional areas on the graph. Due to

constrains on τ_3 and τ_4 shown in Section 3, the LM ratio chart is bounded, unlike the β_1-β_2 chart. Once the τ_3-τ_4 chart is constructed, the sample L-CK and L-CS can be plotted onto the chart for GOF assessment. Points on or near the line (or region) indicate an adequate fit, whereas those further away indicate a poor fit. Hence, the chart provides a visualization of what distributions are compatible with the data set. Figure 4 (left) shows the LM ratio chart for the BS distribution as a curve on the axes (τ_3, τ_4). When $\alpha \to 0$, we have $\tau_3^{\mathrm{BS}} \to 0$ and $\tau_4^{\mathrm{BS}} \to 0.1226$. These limiting values for τ_3 and τ_4 represent the L-CS and L-CK of the normal distribution, respectively. This is due to the fact that the BS distribution tends to the normal distribution as $\alpha \to 0$. Note that here the LM ratio chart is plotted only for positive values of τ_3, limiting our attention to positively skew distributions. In Figure 4 (left), a curve for the gamma distribution and points representing the EXP and GU distributions have been added for comparison. In the case of the EVBS and EVBS* distributions, the charts contain regions, as seen in Figure 4 (center, right) for $\xi < 1/2$; see equations (12) and (13). Note that, although not shown here, the LM charts for the BSGU and BSGU* distributions contain curves which are subsets of the EVBS and EVBS* regions since, as mentioned before, the former distributions are particular cases of the latter ones.
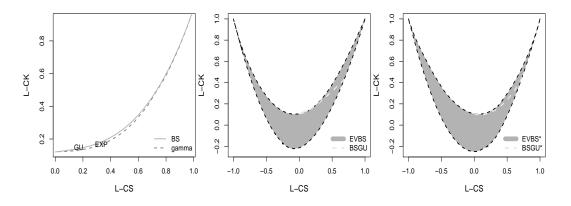

Figure 4. LM ratio charts for BS (left), EVBS (center) and EVBS* (right) distributions.

A second GOF assessment method based on LM is obtained by plotting L-CV versus L-CS, with coordinate axes (τ, τ_3) as defined in equation (8). This is known as the τ-τ_3 chart and it is analogous to the γ-γ_3 chart based on CM [25]. The relation between L-CV (τ) and L-CS (τ_3) is given in general by $\tau = \lambda_1^{-1}\lambda_2^2\lambda_3^{-1}\tau_3$, with λ_1, λ_2 and λ_3 being the 1st, 2nd and 3rd LM given in equation (7), respectively. For the BS distribution, the τ-τ_3 chart is calculated using the relation

$$\tau = \frac{16\pi h_2^2 \tau_3}{\alpha^2(2+\alpha^2)\sqrt{3}},$$

where h_2 is defined in equation (11). In the τ-τ_3 chart, distributions belonging to the location-scale family (for example, the GU distribution) are plotted as a line on the chart. Two-parameter distributions with scale and shape parameters (for example, the BS distribution) generally cover two-dimensional areas on the graph. The τ-τ_3 diagram is not suitable for distributions with location, scale and shape parameters or for distributions with more than one shape parameter (as the GEV and EVBS distributions, respectively), because the set of allowed values covers the whole first quadrant. Figure 5 displays the τ-τ_3 chart for the BS distribution. In this figure, a region for the gamma distribution and lines representing the EXP and GU distributions have been added for comparison. Note that the BS and EXP distributions are contained within the gamma region. Also, observe that both the τ_3-τ_4 and τ-τ_3 charts can be used as a GOF exploratory tool to propose or discard distributions in a global context. However, these charts do not permit formal statistical tests for the distribution identified as appropriate. Some effort along these lines has been conducted using acceptance regions based on LM, but these are beyond the objective of this paper, because goodness of fit assessment is not our main focus. Readers interested in acceptance region for LM are referred to [37], [52] and [54].

When an appropriate distribution is identified by LM charts, we consider a formal GOF test

based on an empirical version of the Kolmogorov-Smirnov (KS) statistic defined by

$$\text{KS} = \max\left\{\max_{1\leq i\leq n}\left\{\frac{i}{n} - U_{i:n}\right\}, \max_{1\leq i\leq n}\left\{U_{i:n} - \frac{i}{n}\right\}\right\}. \tag{14}$$

For details about the KS statistic given in equation (14) and its theoretical properties, see [2]. Then, a third GOF method based on the KS test and the LM estimation method can be obtained based on the idea of probability-probability (PP) plots [4]. In that case, the statistical hypotheses are

H$_0$: "The data are generated from a distribution with CDF F_X"

versus $\hspace{10cm}$ (15)

H$_1$: "The data are not generated from this distribution".

If the CDF hypothesised in (15) is not completely specified in H$_0$, then the corresponding parameters must be estimated consistently. We use the LM method to estimate these parameters and the data are transformed to test normality of the corresponding distribution under H$_0$. The GOF method based on the KS test and the PP plot, with its acceptance bands, is summarized in Algorithm 1. To select the best distribution, we use Algorithm 1 and choose the distribution whose associated KS p-value is maximum. This is equivalent to the Anderson-Darling criterion [22].

Figure 5. τ-τ_3 chart for the indicated distributions.

3.3   *Parameter estimation based on L-moments*

To estimate parameters with the LM method, we use an objective function proposed by [1, 7] given by

$$g(\boldsymbol{\theta}) = \log\left(1 + \sum_{j=2}^{m+1}(l_j - \lambda_j)^2\right), \tag{16}$$

where again $\boldsymbol{\theta}$ is an $m \times 1$ vector of parameters depending of each distribution and λ_j, l_j are defined in equations (7), (9), respectively. Estimation of $\boldsymbol{\theta}$ then involves the minimization of $g(\boldsymbol{\theta})$. The objective function given in equation (16) was chosen by [7] as the standard least squares (LS) solution surface, which can become quite flat far away from the minimum. For the BS distribution, the objective function given in equation (16) is

$$g(\boldsymbol{\theta}) = g(\alpha, \beta) = \log\left(1 + (l_2 - \lambda_2^{\text{BS}})^2 + (l_3 - \lambda_3^{\text{BS}})^2\right). \tag{17}$$

Algorithm 1 GOF test based on KS and LM for BS and EVBS distributions

---

1: Collect and order data $x_1, x_2, \ldots, x_n$ as $x_{1:n}, \ldots, x_{n:n}$.
2: Estimate the parameter $\boldsymbol{\theta}$ of $F_X(x; \boldsymbol{\theta})$ by $\widehat{\boldsymbol{\theta}}$ using LM (see Section 3.3), with $x_1, \ldots, x_n$. Note that $\boldsymbol{\theta}$ is an $m \times 1$ vector of parameters depending of each (BS, EVBS or EVBS*) distribution.
3: Obtain $\widehat{v}_{i:n} = F_X(x_{i:n}; \widehat{\boldsymbol{\theta}})$, for $i = 1, \ldots, n$.
4: Compute $\widehat{y}_i = \Phi^{-1}(\widehat{v}_{i:n})$, where Φ^{-1} is the N(0,1) inverse CDF, for $i = 1, \ldots, n$.
5: Calculate $\widehat{u}_{i:n} = \Phi(\widehat{z}_i)$, with

$$\widehat{z}_i = \frac{\widehat{y}_i - \overline{y}}{s_y}, \quad i = 1, \ldots, n,$$

where

$$\overline{y} = \frac{1}{n}\sum_{i=1}^{n}\widehat{y}_i, \quad s_y = \frac{1}{n-1}\sum_{i=1}^{n}(\widehat{y}_i - \overline{y})^2.$$

6: Sketch the PP plot for $w_{i:n}$ versus $\widehat{u}_{i:n}$, that is, for the pairs

$$\left(\frac{i-0.5}{n}, \Phi\left(\frac{\widehat{y}_i - \overline{y}}{s_y}\right)\right), \quad i = 1, \ldots, n.$$

7: Fix a significance level ζ and construct acceptance bands according to

$$\left(\max\left\{w - d_{1-\zeta} + \frac{1}{2n}, 0\right\}, \min\left\{w + d_{1-\zeta} - \frac{1}{2n}, 1\right\}\right),$$

where w is a continuous version of $w_{i:n} = (i - 0.5)/n$ defined in Step 6, and $d_{1-\zeta}$ is the $100 \times (1 - \zeta)$th quantile of the distribution of the KS statistic defined in (14), with the RV U approximately following a U(0,1) distribution.
8: Determine the p-value of the KS statistic defined in (14), evaluated it at $U_{i:n} = \widehat{u}_{i:n}$, and reject H$_0$ specified in (15) for the significance level fixed in Step 7 based on this p-value.
9: Check agreement between steps 7 and 8, that is, if no points in the PP plot lie outside the acceptance bands, then the p-value must be smaller than or equal to the fixed significance level; otherwise, if at least one point lies outside, the p-value must be greater than the fixed significance level.

Optimization of $g(\boldsymbol{\theta})$ given in equation (17) needs a numeric procedure to attain a solution. We use a quasi-Newton method (implemented by the `optim` command of the R software) with a starting value $\alpha^0 = \sqrt{2(l_1/\text{Me} - 1)}$ for the shape parameter of the BS distribution, where Me is the sample median, and $\beta^0 = \text{Me}$ for its scale parameter. For the EVBS and EVBS* distributions, the objective function given in equation (16) becomes

$$g(\boldsymbol{\theta}) = g(\alpha, \beta, \xi) = \log(1 + \sum_{r=2}^{4}(l_r - \lambda_r^{\text{S}})), \tag{18}$$

where $\text{S} \in \{\text{EVBS}, \text{EVBS}^*\}$. Estimation of parameters for the EVBS and EVBS* distributions with the LM method is a complex problem. Such as in the BS case, optimization of $g(\boldsymbol{\theta})$ given in equation (18) needs a numeric procedure to attain a solution. However, due to the form of the parameter space of the EVBS and EVBS* distributions, an iterative procedure for a constrained non-linear optimization is required. Hence, a variant of a quasi-Newton method, named the Broyden-Fletcher-Goldfarb-Shanno (BFGS) algorithm, which handles constraints and it is denoted by L-BFGS-B, is used to minimise $g(\alpha, \beta, \xi)$ given in equation (18), with $\xi < 1/2$. The command `optim` of the R software, with the option `method = L-BFGS-B`, allows us to obtain the solution of this non-linear constrained optimization problem. To find starting values for the numerical procedure needed for obtaining the LM estimates of the EVBS (or EVBS*) model parameters α and β, one can consider different methods. We use a graphical approach analogous to the probability plot [26]. This approach transforms the data and forms pairs following a line, if these data have the EVBS (or EVBS*) distribution. Then, by means of regression, the slope and intercept of this line are obtained and, through them, starting values for α and β are reached. Algorithm 2 details this graphical approach for the EVBS distribution, with an analogous algorithm for the EVBS* distribution.

Algorithm 2 Approach for initial values in LM estimation of EVBS parameters.

1: Obtain an initial value for ξ by the LM method using the GEV distribution, with the expression

$$\overline{\xi} = \frac{1}{7.8590c + 2.9554c^2},$$

where $c = 2/(7.859c + 2.9554c^2) - \log(2)/\log(3)$, which can be seen in [13].

2: Consider the EVBS CDF given in equation (4) and write

$$x = \beta + \alpha\sqrt{\beta}\sqrt{x}G^{-1}(F_X(x; \alpha, \beta, \xi)),$$

where G^{-1} is the inverse CDF of the associated EV distribution and F_X is the EVBS CDF.

3: Express

$$p = \sqrt{x}G^{-1}(F_X(x)),$$

obtaining the line $v \approx a + bu$, where $v = x$, $a = \beta$ is the intercept, $u = p$ and $b = \alpha\sqrt{\beta}$ is the slope of the line.

4: Collect n data $x_1, \ldots, x_n$ and order them as $x_{1:n} \leq \cdots \leq x_{n:n}$.

5: Approximate $F_X(x_{i:n}; \alpha, \beta, \xi)$ using

$$w_{i:n} = \frac{i - 0.5}{n}, \quad i = 1, \ldots, n.$$

6: Regress $x_{i:n}$ on $\bar{p}_i$, where $\bar{p}_i = \sqrt{x_{i:n}}G^{-1}(w_{i:n})$, which will result in an approximate line if the data follow an EVBS distribution.

7: Estimate the α parameter of the EVBS distribution with the LS method for the regression of $x_{i:n}$ on $\bar{p}_i$, obtaining $\bar{\alpha} = \bar{b}/\sqrt{\bar{a}}$, where $\bar{a}$ and $\bar{b}$ are the estimated slope and intercept of the corresponding regression, respectively. The parameter β is estimated by $\bar{\beta} = \bar{a}$.

From the asymptotic distribution of the LM estimator, $\widehat{\boldsymbol{\theta}}$ say, of the $m \times 1$ vector of parameters $\boldsymbol{\theta}$ mentioned in [13], as $n \to \infty$, we have that

$$\sqrt{n}(\widehat{\boldsymbol{\theta}} - \boldsymbol{\theta}) \xrightarrow{\mathcal{D}} \mathrm{N}_m(\mathbf{0}_{m\times 1}, \boldsymbol{\Sigma}(\boldsymbol{\theta})), \tag{19}$$

where $\xrightarrow{\mathcal{D}}$ denotes convergence in distribution, $\mathbf{0}_{m\times 1}$ is an $m \times 1$ vector of zeros, and $\boldsymbol{\Sigma}(\boldsymbol{\theta})$ is the asymptotic variance-covariance matrix of $\widehat{\boldsymbol{\theta}}$, which exists, is non-singular and can be obtained using the bootstrap method [8, 51]. Thus, based on the asymptotic distribution defined in (19), an approximate $100 \times (1 - \zeta)\%$ confidence region for $\boldsymbol{\theta}$ is

$$(\widehat{\boldsymbol{\theta}} - \boldsymbol{\theta})^{\top}(\widehat{\boldsymbol{\Sigma}}_{\mathrm{B}}(\boldsymbol{\theta}))^{-1}(\widehat{\boldsymbol{\theta}} - \boldsymbol{\theta}) \leq \chi^2_{1-\zeta}(m), \quad \boldsymbol{\theta} \in \mathrm{R}^m, \quad 0 < \zeta < 1,$$

where $\chi^2_{1-\zeta}(m)$ is the $100 \times (1 - \zeta)$th quantile of the χ^2 distribution with m degrees of freedom and $\widehat{\boldsymbol{\Sigma}}_{\mathrm{B}}(\boldsymbol{\theta})$ is the bootstrap estimates of $\boldsymbol{\Sigma}(\boldsymbol{\theta})$. Note that $m = 2$ for BS and BSGU distributions and $m = 3$ for EVBS and EVBS* distributions, with $\xi \neq 0$.

It is of interest to compare the LM and maximum likelihood (ML) estimation methods. Results for the asymptotic variance and bias of the LM and ML estimators based on MC simulations for the GEV distribution are discussed in [13, pp. 41-43]. They mention that the LM estimator is efficient in relation to the ML estimator. Similar results are obtained for asymmetric exponential power, generalized Pareto and mixture Weibull distributions, as mentioned in [7],[13], and [16], respectively. We conduct an MC simulation study to verify this efficiency in the cases the BS and EVBS distributions, with results reported in Section 4.

4. Empirical results

In this section, we provide the numerical results of our study. First, we check some properties of the LM and ML estimators for the BS and EVBS distribution parameters. Second, we apply the derived GOF and estimation methods to real-world earthquake data.

4.1   *Simulation*

An MC simulation is carried out to evaluate the performance of the LM estimators for the BS and EVBS distributions. We consider samples of size $n \in \{10, 100\}$, corresponding to small and large samples, and 1000 MC replicates. For the BS distribution, we assume, without loss of generality, that $\beta = 1.0$ because it is a scale parameter, whereas its shape parameter is considered as $\alpha \in \{0.2, 1.0\}$, related to low and moderate asymmetry, respectively. For the EVBS distribution, our interest is in its right-tail parameter, so we take $\alpha = 0.2$, $\beta = 1.0$ and $\xi \in \{-0.2, 0.0, 0.2\}$, associated with a light tail (Weibull domain of attraction), an EXP tail (Gumbel domain of attraction) and a heavy tail (Fréchet domain of attraction), respectively. We compute the empirical mean and SE of the parameter estimators from both LM and ML methods; for more details of ML estimators for BS and EVBS distributions, see [3, 31] and [9], respectively. In addition, we compute the bias and root mean squared error (RMSE) –defined as the square root of the mean squared error– of the LM estimators, as well as the coverage probability (CP) of 95% confidence intervals for the corresponding parameter. Using these results, we study empirically the statistical properties of the LM estimators mentioned at the end of Section 3. Tables 1 and 2, and Figure 6 show that the already mentioned properties of the LM estimators are true, empirically (a theoretical study is beyond the objective of the paper). In general, note that the LM estimators are more efficient than the ML estimators. In the case of the BS distribution, the LM estimator is slightly more efficient than the ML estimator when α is small. In addition, when α increases, the bias increases too, whereas the difference between both estimators is again insignificant. Observe that the CPs are very close to 95% for both of the BS and EVBS distributions, when $n = 100$ for LM and ML methods. To investigate convergence to normality of the LM estimator of ξ empirically, we show PP plots with 95% acceptance bands (according to Algorithm 1) in Figure 6 for a sample size equal to $n = 100$. Note that this normality is supported empirically when ξ is positive, zero and negative, that is, for all the domains of attraction.

Table 1.   Empirical mean, SE, bias, RMSE and CPs (95%) for the BS distribution based on MC simulations.

n	Parameter	Mean$_{\text{LM}}$ (SE)	Bias$_{\text{LM}}$	RMSE$_{\text{LM}}$	CP$_{\text{LM}}$(%)	Mean$_{\text{ML}}$ (SE)	Bias$_{\text{ML}}$	RMSE$_{\text{ML}}$	CP$_{\text{ML}}$(%)
10	$\alpha = 0.2$	0.199 (0.030)	-0.001	0.030	95.6	0.184 (0.043)	-0.016	0.046	95.2
	$\beta = 1.0$	0.999 (0.061)	-0.001	0.061	94.9	1.003 (0.064)	0.003	0.064	94.9
	$\alpha = 1.0$	0.972 (0.305)	-0.028	0.306	95.5	0.915 (0.217)	-0.085	0.233	95.2
	$\beta = 1.0$	0.978 (0.171)	-0.022	0.172	94.7	1.045 (0.300)	0.045	0.303	95.3
100	$\alpha = 0.2$	0.199 (0.014)	-0.001	0.014	94.9	0.198 (0.015)	-0.002	0.015	94.3
	$\beta = 1.0$	1.000 (0.019)	0.000	0.019	95.3	1.000 (0.020)	0.000	0.020	95.4
	$\alpha = 1.0$	0.994 (0.096)	-0.006	0.096	95.0	0.988 (0.069)	-0.012	0.070	94.9
	$\beta = 1.0$	0.998 (0.050)	-0.002	0.050	95.2	1.005 (0.089)	0.005	0.089	95.5

Table 2.   Empirical mean, SE, bias, RMSE and CPs (95%) for the EVBS distribution based on MC simulations.

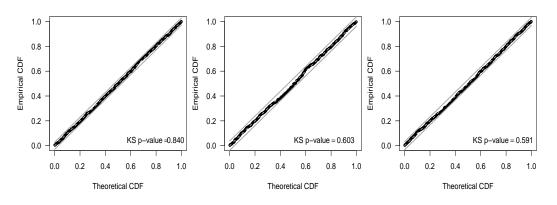| n	Parameter	Mean$_{\text{LM}}$ (SE)	Bias$_{\text{LM}}$	RMSE$_{\text{LM}}$	CP$_{\text{LM}}$(%)	Mean$_{\text{ML}}$ (SE)	Bias$_{\text{ML}}$	RMSE$_{\text{ML}}$	CP$_{\text{ML}}$(%)
	$\alpha = 1.0$	0.960 (0.251)	-0.040	0.254	96.0	0.947 (0.328)	-0.053	0.332	96.5
10	$\beta = 1.0$	1.010 (0.370)	0.010	0.370	97.2	1.243 (0.511)	0.243	0.566	95.6
	$\xi = -0.25$	-0.237 (0.194)	0.013	0.194	96.6	-0.445 (0.370)	-0.195	0.418	96.5
	$\alpha = 1.0$	1.002 (1.135)	0.002	1.135	99.9	0.973 (1.188)	-0.027	1.199	99.7
	$\beta = 1.0$	1.033 (0.412)	0.033	0.413	95.3	1.316 (1.001)	0.316	1.049	97.5
	$\xi = 0.0$	-0.050 (0.209)	-0.060	0.217	97.4	-0.101 (0.632)	-1.101	0.640	96.3
	$\alpha = 1.0$	0.997 (0.901)	-0.003	0.901	99.7	0.961 (0.942)	-0.039	0.889	99.7
	$\beta = 1.0$	1.121 (0.497)	0.121	0.512	98.5	1.223 (0.675)	0.223	0.719	95.2
	$\xi = 0.25$	0.150 (0.225)	0.100	0.246	99.9	0.163 (0.672)	-0.087	0.678	95.4
	$\alpha = 1.0$	0.993 (0.079)	-0.007	0.079	95.0	0.993 (0.077)	-0.007	0.077	94.2
100	$\beta = 1.0$	1.021 (0.106)	0.021	0.108	95.7	1.020 (0.107)	0.020	0.109	95.0
	$\xi = -0.25$	-0.267 (0.073)	-0.017	0.075	95.1	-0.268 (0.074)	-0.018	0.076	95.0
	$\alpha = 1.0$	0.982 (0.081)	-0.018	0.083	94.1	0.985 (0.080)	-0.015	0.081	94.5
	$\beta = 1.0$	0.977 (0.100)	-0.023	0.103	94.5	0.982 (0.102)	-0.018	0.104	94.7
	$\xi = 0.0$	0.034 (0.070)	0.034	0.077	94.7	0.036 (0.086)	0.036	0.093	94.5
	$\alpha = 1.0$	0.993 (0.119)	-0.007	0.119	95.2	0.989 (0.105)	-0.011	0.105	94.5
	$\beta = 1.0$	1.054 (0.126)	0.054	0.137	95.0	1.017 (0.116)	0.017	0.117	95.7
	$\xi = 0.25$	0.243 (0.070)	-0.007	0.070	96.0	0.237 (0.094)	-0.013	0.095	95.6

Figure 6. PP plots with 95% acceptance bands for the distribution of the EVBS right-tail index estimator with $\xi = -0.25$ (left), $\xi = 0$ (center) and $\xi = 0.25$ (right).

4.2   *Analysis of annual maximum data*

A statistical analysis of annual maximum earthquake magnitudes using LM methods is performed with data of these magnitudes within a one year period. We implement the theoretical results obtained in this paper in the R software and the corresponding codes, as well as data, are available from the authors upon request. The measurements of magnitude are on the moment magnitude scale (M_w), abbreviated sometimes also as MMS, MW or simply M [15, 46]. The M_w scale is used by seismologists to quantify the size of an earthquake through the energy released. The magnitude corresponds to the seismic moment of the earthquake and it is equal to the rigidity of the Earth multiplied by the mean quantity of slip on the fault and the size of the slipped area. This scale is often confused with the Richter magnitude scale, even though their formulas are different. The M_w scale is used to establish magnitudes for all modern large earthquakes by the United States Geological Survey. The data set used in this work is obtained from the Incorporate Research Institute for Seismology (http://ds.iris.edu), which collects earthquakes magnitude data from the GCMT server (http://www.globalcmt.org). In particular, we consider data from 07-March-1962 to 25-February-2015 assigned to 50 seismic zones as proposed by [11]; referred to as Flinn-Engdalh (FE) seismic zones. The annual maximum earthquake magnitudes are displayed as a map in Figure 7.
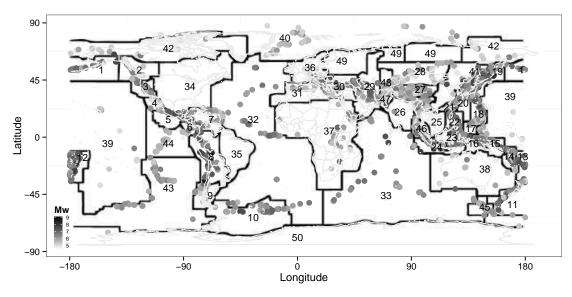

Figure 7. Planisphere plot based on earthquake catalogue data of annual maximum magnitudes and FE seismic zones.

An exploratory data analysis is performed, and then the LM-based methods are used for GOF assessment and parameter estimation. Table 3 provides a summary of the annual maximum M_w for each FE zone. This table includes the zone name and number (ID from 1 to 48) and sample values of the minimum $(x_{1:n})$, Me, mean $(\bar{x})$, SD, CS, CK, L-CV, L-CS, L-CK and maximum $(x_{n:n})$. Figure 8 shows the adjusted box plots for asymmetric data of annual maximum magnitudes for each FE zone, which can be constructed by the command adjbox of the robustbase package in the R software [42]. We only consider zones with more than 10 events. Note that the magnitudes follow a positively skewed distribution (CS > 0, L-CS > 0) and L-CV close to zero in most zones, with a few outliers in some zones and a high kurtosis in several zones.

Table 3. Descriptive summary of annual maximum earthquake magnitude data.

Zone	ID	n	$x_{1:n}$	Me	$\bar{x}$	CV	CS	CK	L-CV	L-CS	L-CK	$x_{n:n}$
Alaska, Aleutian Arc	1	39	5.70	6.80	6.86	0.080	0.37	2.68	0.045	0.10	0.15	7.90
Southeastern Alaska to Washington	2	33	5.20	6.00	6.16	0.106	0.69	2.80	0.060	0.16	0.08	7.80
Oregon, California and Nevada	3	39	5.50	6.20	6.24	0.091	0.43	1.88	0.053	0.14	-0.01	7.30
Baja California and Gulf of California	4	32	5.00	5.85	5.94	0.082	0.48	2.42	0.047	0.15	0.08	7.00
Mexico and Guatemala	5	40	5.80	6.70	6.77	0.083	0.41	2.31	0.048	0.11	0.05	8.00
Central America	6	40	5.90	6.50	6.63	0.077	0.60	2.30	0.044	0.16	0.08	7.70
Caribbean Loop	7	39	5.50	6.10	6.23	0.079	0.61	2.69	0.045	0.14	0.11	7.40
Andean South America	8	50	6.30	7.10	7.16	0.082	0.70	2.88	0.046	0.16	0.11	8.80
Extreme South America	9	31	5.00	5.90	5.89	0.071	-0.18	2.20	0.041	-0.05	0.04	6.70
Southern Antilles	10	39	5.90	6.40	6.53	0.072	0.78	2.99	0.041	0.18	0.08	7.80
New Zealand	11	39	5.30	6.70	6.56	0.113	0.11	2.21	0.066	0.02	0.06	8.10
Kermadec, Tonga, Samoa Basin	12	46	6.40	7.05	7.10	0.065	0.41	2.30	0.038	0.10	0.08	8.10
Fiji Islands	13	44	5.90	6.60	6.71	0.066	0.55	2.49	0.037	0.15	0.11	7.70
Vanuatu Islands	14	43	6.30	7.10	7.07	0.052	0.25	2.59	0.030	0.06	0.12	7.90
Bismarck and Solomon Islands	15	40	6.20	7.10	7.08	0.062	0.23	2.42	0.036	0.05	0.06	8.10
New Guinea	16	40	5.90	6.80	6.81	0.070	0.57	3.28	0.040	0.11	0.11	8.20
Caroline Islands	17	39	5.10	5.90	5.95	0.077	0.66	2.68	0.044	0.18	0.11	7.00
Guamto Japan	18	43	5.90	6.60	6.72	0.070	0.17	2.31	0.040	0.05	0.08	7.70
Japan, Kuril Islands, Kamchatka Peninsula	19	42	6.20	7.10	7.15	0.092	0.75	3.23	0.052	0.15	0.10	9.10
Southwestern Japan and Ryukyu Islands	20	39	5.20	6.10	6.24	0.074	-0.01	2.39	0.043	0.02	0.09	7.10
Taiwan	21	38	5.70	6.40	6.46	0.071	0.54	2.68	0.041	0.12	0.12	7.60
Philippine Islands	22	41	5.90	6.90	6.92	0.066	0.03	2.77	0.038	0.01	0.12	8.00
Bornea, Sulawesi	23	41	5.90	6.90	6.84	0.076	0.17	2.10	0.044	0.04	0.05	7.90
Sunda Arc	24	48	6.20	7.00	7.00	0.079	0.67	2.89	0.044	0.14	0.08	8.50
Myanmar and Southeast Asia	25	39	5.20	5.90	5.99	0.083	0.60	2.39	0.047	0.17	0.05	7.20
India, Xizand, Sichuan, Yunnan	26	37	5.20	6.20	6.25	0.091	0.94	4.04	0.050	0.17	0.21	7.90
Southern Xinjiang to Gansu	27	34	5.40	6.10	6.10	0.089	1.07	4.32	0.048	0.18	0.17	7.80
LakeIssyk-Kulto Lake Baykal	28	31	5.10	5.60	5.78	0.095	0.94	2.88	0.053	0.27	0.09	7.20
Western Asia	29	39	5.10	6.50	6.39	0.097	-0.11	2.40	0.056	-0.03	0.11	7.70
Middle East, Crimea, Eastern Balkans	30	39	5.30	6.40	6.42	0.081	0.10	2.62	0.047	0.00	0.10	7.60
Western Mediterranean Zone	31	37	5.00	5.80	5.84	0.084	0.63	3.12	0.047	0.12	0.17	7.10
Atlantic Ocean	32	39	5.80	6.50	6.51	0.055	-0.14	1.97	0.032	-0.04	0.02	7.10
Indian Ocean	33	40	5.90	6.40	6.52	0.066	1.40	5.13	0.035	0.25	0.26	7.90
Eastern North America	34	16	5.20	5.65	5.83	0.103	1.15	2.97	0.055	0.34	0.17	7.10
Northwestern Europe	36	7	5.10	5.30	5.55	0.094	0.99	2.35	0.052	0.46	0.19	6.50
Africa	37	36	5.10	5.95	6.00	0.087	0.45	2.74	0.050	0.09	0.12	7.20
Australia	38	8	4.90	5.50	5.61	0.094	0.66	2.65	0.055	0.22	0.26	6.60
Pacific Basin	39	21	5.10	5.50	5.72	0.094	0.77	2.32	0.054	0.23	0.08	6.80
Arctic Zone	40	38	5.20	5.65	5.77	0.071	0.88	2.65	0.039	0.25	0.10	6.70
Eastern Asia	41	40	5.60	6.55	6.57	0.107	0.43	2.29	0.061	0.11	0.03	8.30
Northeastern Asia	42	23	5.10	5.40	5.76	0.113	1.13	3.69	0.061	0.30	0.09	7.60
Southeastern and Antarctic Pacific Ocean	43	39	5.80	6.30	6.31	0.043	0.79	3.71	0.024	0.15	0.21	7.10
Galapagos Islands	44	37	5.30	5.90	5.86	0.036	-0.17	3.22	0.021	-0.04	0.13	6.40
Macquarie Loop	45	40	5.70	6.05	6.17	0.068	2.49	11.9	0.033	0.29	0.24	8.10
Andaman Islands to Sumatra	46	39	5.50	6.20	6.48	0.130	1.49	4.59	0.067	0.36	0.20	9.00
Baluchistan	47	24	5.10	5.60	5.86	0.123	1.45	4.33	0.064	0.35	0.20	7.80
Hindu Kushand Pamir	48	40	4.90	6.25	6.29	0.083	0.13	3.50	0.046	0.05	0.19	7.40
Annual maximum series for all zones	-	54	7.00	7.80	7.85	0.061	0.43	2.94	0.034	0.08	0.14	9.10

Figure 8. The adjusted box plots for annual maximum magnitudes of the indicated FE seismic zones.
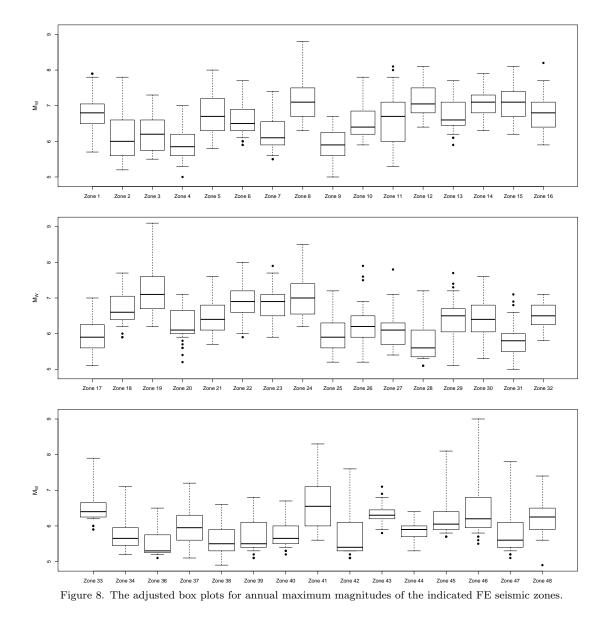
Figure 9 displays LM charts, where each plotted point is the sample LM pair from Table 3 corresponding to an FE zone indicated by its ID in this table. Figure 9 (left) provides the LM ratio chart. From this figure note that 71% of the points are below the GEV curve and inside the EVBS region. Therefore, the GEV and EVBS distributions (and their GU and BSGU special cases) seem to be good candidates for modelling the data. Figure 9 (center, right) presents the LM ratio and τ-τ_3 charts, respectively, for the BS, EXP, gamma and GU distributions. Observe that the non-EV distributions (BS, EXP, gamma) are unsuitable in most of the zones, and even the GU distribution (which is an EV model) is also inadequate as a candidate to describe most of the zones. As illustration, we compute the LM estimates to identify a suitable distribution in the Andean South America (Zone 8), which has the highest frequency of earthquakes. Table 4 provides the estimated parameters for the annual maximum magnitudes. We use the p-value of the KS test and the PP plot with 95% acceptance bands to test the fit of each distribution to the data; see Figure 10. Note that four distributions have been identified as candidates and they are confirmed as suitable by this figure because all points are inside the bands. From Table 4, observe that the best fit corresponds to the BSGU distribution, indicating that it is the most appropriate model to describe annual maximum earthquakes in the Andean South America zone, to which Chile belongs, one of the countries around the world that is more exposed to earthquakes. In statistics, Akaike (AIC) and Bayesian (BIC) information criteria are often used, which allows us to compare

16

and select models. These criteria are given by $\text{AIC} = 2m - 2\ell(\widehat{\boldsymbol{\theta}})$ and $\text{BIC} = m\log(n) - 2\ell(\widehat{\boldsymbol{\theta}})$, where $\ell(\widehat{\boldsymbol{\theta}})$ is the log-likelihood of the model with parameter $\boldsymbol{\theta}$ evaluated at $\widehat{\boldsymbol{\theta}}$, n is the sample size and m is the parameter number. For more details about AIC and BIC, see [26] and references therein. Table 4 also provides AIC and BIC for the data under analysis, whose criteria indicate again that the BSGU distribution is the best model to describe annual maximum earthquakes in the Andean South America zone.
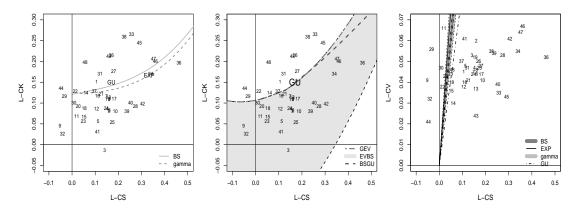

Figure 9. LM ratio chart for BS, EXP, gamma and GU distributions (left), LM ratio chart for BSGU, EVBS, GEV and GU distributions (center), and τ-τ_3 chart for BS, EXP, gamma and GU distributions (right) with data of annual maximum magnitudes in the Andean South America zone.

Table 4. Estimated parameters, KS p-value, AIC and BIC for data of annual maximum magnitudes in the Andean South America zone.

Distribution	Parameter estimates				KS p-value	AIC	BIC
	Location	Shape	Scale	Right tail index			
$\text{EVBS}(\alpha, \beta, \xi)$	-	0.069	6.885	-0.065	0.457	87.9	93.6
$\text{GEV}(\mu, \sigma, \xi)$	6.888	-	0.486	-0.013	0.405	88.3	94.1
$\text{BSGU}(\alpha, \beta) \equiv \text{EVBS}(\alpha, \beta, 0)$	-	0.066	6.872	-	0.572	83.4	87.2
$\text{GU}(\mu, \sigma) \equiv \text{GEV}(\alpha, \sigma, 0)$	6.886	-	0.480	-	0.458	85.9	89.6

5. Conclusions and future work

In this work, L-moment methods based on the Birnbaum-Saunders distribution and its extreme value version have been derived, implemented and applied. These L-moments were used to obtain estimators of the model parameters and to provide goodness-of-fit methods allowing the selection of an appropriate distribution for a given data set. In addition, Monte Carlo simulations were used to show that the L-moment estimators have a good performance and are, in general, more efficient than the corresponding maximum likelihood estimators. Furthermore, the asymptotic normality of the L-moment estimators was demonstrated empirically. The proposed methods were applied to a seismic data set taken from the global centroid moment tensor catalogue, for the period between 07-March-1962 and 25-February-2015. With these data, an analysis of earthquake annual maximum magnitudes was performed. It allowed us to conclude that some extreme value Birnbaum-Saunders models, known as the Birnbaum-Saunders-Gumbel model, are appropriate distributions for describing the behaviour of maximum seismic events and have a better performance than the classic extreme value distributions. Thus, extreme value Birnbaum-Saunders models could be useful alternatives to the more commonly used distributions, such as the exponential, generalized extreme value and gamma models. We think that the Birnbaum-Saunders distributions can also be considered in the modelling of earthquake data in highly seismic zones, such as California, Chile and Japan, which may allow the authorities to produce more reliable earthquake hazard maps.
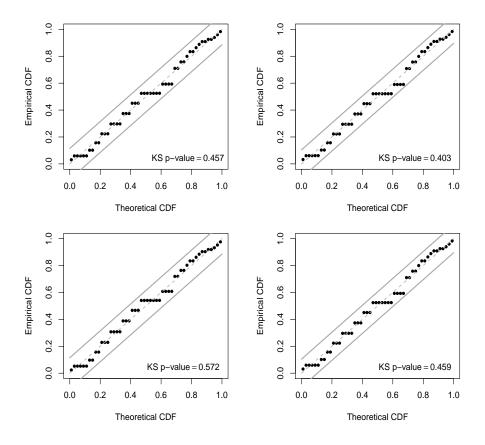
Figure 10. PP plots with 95% acceptance bands for EVBS (top-left), GEV (top-right), BSGU (bottom-left) and GU (bottom-right) distributions with data of annual maximum magnitudes in the Andean South America zone.

Certain return periods (for example, 10-year and 100-year) are usually considered in similar studies to that presented in the present paper [5, p. 62]. Furthermore, acceptance regions for goodness of fit based on L-moments are also an important issue to be considered [52]. Incorporation of censored data, multivariate versions of value extreme Birnbaum-Saunders distributions, and their modeling and diagnostics are also of interest [39, 40] in the context of L-moments. As future research, all of these issues are being explored by the authors.

Acknowledgement

References

[1] Asquith, W. (2014). Parameter estimation for the 4-parameter asymmetric exponential power distribution by the method of L-moments using R. *Computational Statistics and Data Analysis*, 71:955–970.

[2] Barros, M., Leiva, V., Ospina, R., and Tsuyuguchi, A. (2014). Goodness-of-fit tests for the Birnbaum-Saunders distribution with censored reliability data. *IEEE Transactions on Reliability*, 63:543–554.

[3] Birnbaum, Z. W. and Saunders, S. C. (1969). Estimation for a family of life distributions with applications to fatigue. *Journal of Applied Probability*, 6:328–347.

[4] Castro-Kuriss, C., Leiva, V., and Athayde, E. (2014). Graphical tools to assess goodness-of-fit in non-location-scale distributions. *Revista Colombiana de Estadística*, 37:341–365.

[5] Coles, S. (2001). *An Introduction to Statistical Modeling of Extreme Values*. Springer, London, UK.

[6] de Haan, L. and Ferreira, A. (2006). *Extreme Value Theory: An Introduction*. Springer, New York, US.

[7] Delicado, P. and Goria, M. (2008). A small sample comparison of maximum likelihood, moments and L-moments methods for the asymmetric exponential power distribution. *Computational Statistics and Data Analysis*, 52:1661–1673.

[8] Efron, B. (1981). Censored data and the bootstrap. *Journal of the American Statistical Association*, 76:312 – 319.

[9] Ferreira, M., Gomes, M. I., and Leiva, V. (2012). On an extreme value version of the Birnbaum-Saunders distribution. *REVSTAT Statistical Journal*, 10:181–210.

[10] Fierro, R. and Leiva, V. (2016). A stochastic methodology for risk assessment of a large earthquake when a long time has elapsed. *Stochastic Environmental Research and Risk Assessment*, pages in press available at `http://dx.doi.org/10.1007/s00477--016--1288--5`.

[11] Flinn, E. and Engdahl, E. (1965). A proposed basis for geographical and seismic regionalization. *Reviews of Geophysics*, 3:123–149.

[12] Garcia-Papani, F., Uribe-Opazo, M., Leiva, V., and Aykroyd, R. (2016). Birnbaum-Saunders spatial modelling and diagnostics applied to agricultural engineering data. *Stochastic Environmental Research and Risk Assessment*, pages in press available at `http://dx.doi.org/10.1007/s00477--015--1204--4`.

[13] Hosking, J. and Wallis, J. (1997). *Regional Frequency Analysis: An Approach Based on L-moments*. Cambridge Press, New York, US.

[14] Johnson, N., Kotz, S., and Balakrishnan, N. (1995). *Continuous Univariate Distributions*, volume 2. Wiley, New York, US.

[15] Kagan, Y. (1997). Seismic moment-frequency relation for shallow earthquakes: Regional comparison. *Journal of Geophysical Research*, 102:28–35.

[16] Karakoca, A., Erisoglu, U., and Erisoglu, M. (2015). A comparison of the parameter estimation methods for bimodal mixture weibull distribution with complete data. *Journal of Applied Statistics*, 42:1472–1489.

[17] Karvanen, J. (2006). L-moments and quantile mixtures. *Computational Statistics and Data Analysis*, 51:947–959.

[18] Karvanen, J. (2016). *Lmoments: L-moments and quantile mixtures*. R package version 1.2-3.

[19] Kim, D., Kim, B., Lee, S., and Cho, Y. (2014). Best-fit distribution and log-normality for tsunami heights along coastal lines. *Stochastic Environmental Research and Risk Assessment*, 28:881–893.

[20] Kotz, S., Leiva, V., and Sanhueza, A. (2010). Two new mixture models related to the inverse Gaussian distribution. *Methodology and Computing in Applied Probability*, 12:199–212.

[21] Kyselý, J. and Picek, J. (2007). Regional growth curves and improved design value estimates of extreme precipitations event in the Czech Republic. *Climate Research*, 33:243–255.

[22] Laio, F., Baldassarre, G., and Montanari, A. (2009). Model selection techniques for the frequency analysis of hydrological extremes. *Water Resources Research*, 45:1–11.

[23] Leao, J., Leiva, V., Saulo, H., and Tomazella, V. (2017). Birnbaum-Saunders frailty regression models: Diagnostics and application to medical data. *Biometrical Journal*, page in press available at `http://dx.doi.org/10.1002/bimj.200800143`.

[24] Leiva, V., Athayde, E., Azevedo, C., and Marchant, C. (2011). Modeling wind energy flux by a Birnbaum-Saunders distribution with unknown shift parameter. *Journal of Applied Statistics*, 38:2819–2838.

[25] Leiva, V., Barros, M., Paula, G., and Sanhueza, A. (2008a). Generalized Birnbaum-Saunders distribution applied to air pollutant concentration. *Environmetrics*, 19:235–249.

[26] Leiva, V., Ferreira, M., Gomes, M. I., and Lillo, C. (2016a). Extreme value Birnbaum-Saunders regression models applied to environmental data. *Stochastic Environmental Research and Risk Assessment*, 30:1045–1058.

[27] Leiva, V., Marchant, C., Ruggeri, F., and Saulo, H. (2015a). A criterion for environmental assessment using Birnbaum-Saunders attribute control charts. *Environmetrics*, 26:463–476.

[28] Leiva, V., Marchant, C., Saulo, H., Aslam, M., and Rojas, F. (2014a). Capability indices for Birnbaum-Saunders processes applied to electronic and food industries. *Journal of Applied Statistics*, 41:1881–1902.

[29] Leiva, V., Rojas, E., Galea, M., and Sanhueza, A. (2014b). Diagnostics in Birnbaum-Saunders accelerated life models with an application to fatigue data. *Applied Stochastic Models in Business and Industry*, 30:115–131.

[30] Leiva, V., Ruggeri, F., Saulo, H., and Vivanco, J. F. (2017). A methodology based on the Birnbaum-Saunders distribution for reliability analysis applied to nano-materials. *Reliability Engineering and System Safety*, 157:192–201.

[31] Leiva, V., Sanhueza, A., Sen, P., and Paula, G. (2008b). Random number generators for the generalized Birnbaum-Saunders distribution. *Journal of Statistical Computation and Simulation*, 78:1105–1118.

[32] Leiva, V., Santos-Neto, M., Cysneiros, F. J. A., and Barros, M. (2014c). Birnbaum-Saunders statistical modelling: A new approach. *Statistical Modelling*, 14:21–48.

[33] Leiva, V., Santos-Neto, M., Cysneiros, F. J. A., and Barros, M. (2016b). A methodology for stochastic inventory models based on a zero-adjusted Birnbaum-Saunders distribution. *Applied Stochastic Models in Business and Industry*, 32:74–89.

[34] Leiva, V. and Saunders, S. C. (2015). Cumulative damage models. *Wiley StatsRef: Statistics Reference Online (available at http: // dx. doi. org/ 10. 1002/ 9781118445112. stat02136. pub2)*, pages 1–10.

[35] Leiva, V., Tejo, M., Guiraud, P., Schmachtenberg, O., Orio, P., and Marmolejo, F. (2015b). Modeling neural activity with cumulative damage distributions. *Biological Cybernetics*, 109:421–433.

[36] Li, X., Zuo, Y., Zhuang, X., and Zhu, H. (2013). Estimation of fracture trace length distributions using probability weighted moments and L-moments. *Engineering Geology*, 168:69–85.

[37] Liou, J.-J., Wu, Y.-C., and Cheng, K.-S. (2008). Establishing acceptance regions for L-moments based goodness-of-fit tests by stochastic simulation. *Journal of Hydrology*, 355:49–62.

[38] Marchant, C., Leiva, V., Cavieres, M., and Sanhueza, A. (2013). Air contaminant statistical distributions with application to PM10 in Santiago, Chile. *Reviews of Environmental Contamination and Toxicology*, 223:1–31.

[39] Marchant, C., Leiva, V., and Cysneiros, F. J. A. (2016a). A multivariate log-linear model for Birnbaum-Saunders distributions. *IEEE Transactions on Reliability*, 65:816–827.

[40] Marchant, C., Leiva, V., Cysneiros, F. J. A., and Vivanco, J. F. (2016b). Diagnostics in multivariate generalized Birnbaum-Saunders regression models. *Journal of Applied Statistics*, 43:2829–2849.

[41] Nicolis, O., Chiodi, M., and Adelfio, G. (2015). Windowed ETAS models with application to the Chilean seismic catalogs. *Spatial Statistics*, 14:151–165.

[42] Rousseeuw, P., Croux, C., Todorov, V., Ruckstuhl, A., Salibian-Barrera, M., Verbeke, T., Koller, M., and Maechler, M. (2015). *robustbase: Basic robust statistics*. R package version 0.92-5.

[43] Santos-Neto, M., Cysneiros, F. J. A., Leiva, V., and Barros, M. (2016). Reparameterized Birnbaum-Saunders regression models with varying precision. *Electronic Journal of Statistics*, 10:2825–2855.

[44] Saulo, H., Leiva, V., Ziegelmann, F. A., and Marchant, C. (2013). A nonparametric method for estimating asymmetric densities based on skewed Birnbaum-Saunders distributions applied to environmental data. *Stochastic Environmental Research and Risk Assessment*, 27:1479–1491.

[45] Thompson, E., Baise, L., and Vogel, R. (2007). A global index earthquake approach to probabilistic assessment of extremes. *Journal of Geophysical Research*, 112:1–12.

[46] Thompson, E., Hewlett, J., Baise, L., and Vogel, R. (2011). The Gumbel hypothesis test for left censored observations using regional earthquake records as an example. *Natural Hazards and Earth System Sciences*, 11:115–126.

[47] Ulrych, T., Velis, D., Woodbury, A., and Sacchi, M. (2000). L-moments and C-moments. *Stochastic Environmental Research and Risk Assessment*, 14:50–68.

[48] Unnikrishnan, N. and Vineshkumar, B. (2010). L-moments of residual life. *Journal of Statistical Planning and Inference*, 140:2618–2631.

[49] Vilca, F., Sanhueza, A., Leiva, V., and Christakos, G. (2010). An extended Birnbaum-Saunders model and its application in the study of environmental quality in Santiago, Chile. *Stochastic Environmental Research and Risk Assessment*, 24:771–782.

[50] Vogel, R. (1995). Recent advances and themes in hydrology. *Reviews of Geophysics*, 33:933–936.

[51] Wang, D., Hutson, A., and Miecznikowsky, J. (2014). L-moment estimation for parametric survival models given censored data. *Statistical Methodology*, 7:655–667.

[52] Wang, M., Zhao, J., Sun, X., and Park, C. (2013). Robust explicit estimation of the two-parameter Birnbaum-Saunders distribution. *Journal of Applied Statistics*, 40:2259–2274.

[53] Wanke, P. and Leiva, V. (2015). Exploring the potential use of the Birnbaum-Saunders distribution in inventory management. *Mathematical Problems in Engineering*, Article ID 827246:1–9.

[54] Wu, Y.-C., Liou, J.-J., Su, Y.-F., and Cheng, K.-S. (2012). Establishing acceptance regions for L-moments based goodness-of-fit tests for the Pearson type III distribution. *Stochastic Environmental Research and Risk Assessment*, 26:873–885.